Journal of Volcanology and Geothermal Research 188 (2009) 297–304

Contents lists available at ScienceDirect

Journal of Volcanology and Geothermal Research

journal homepage: www.elsevier.com/locate/jvolgeores

Recent magmatotectonic activity in the Eastern Snake River Plain–Island Park region revealed by SAR interferometry

M.H. Aly *, D.W. Rodgers, G.D. Thackray, S.S. Hughes

Department of Geosciences, Idaho State University, Pocatello, Idaho 83209-8072, United States

ARTICLE INFO

Article history:
Received 19 May 2008
Accepted 20 May 2009
Available online 6 June 2009

Keywords:
Eastern Snake River Plain
Island Park
Yellowstone
Synthetic Aperture Radar Interferometry
crustal deformation
magmatic processes

ABSTRACT

Synthetic Aperture Radar Interferometry (InSAR) has been applied in this study to address crustal deformation in a 10,000-km^2 region located immediately west of the Yellowstone hotspot. InSAR results show that surface movements in the study area were non-linear and episodic during the period of observation (1993–2006). The Island Park region and its adjacent Eastern Snake River Plain (ESRP) were characterized by northeast-trending zones of uplift ($+1$ cm yr^{-1}) and subsidence (-1 cm yr^{-1}) with various extents through time. The western edge of Yellowstone caldera experienced episodes of subsidence (-1 cm yr^{-1}) during 1997–2000 and uplift ($+3$ cm yr^{-1}) during 2004–2006. Differential surface movements of varying rates were also detected between 1993 and 2006 in the vicinity of Basin and Range normal faults to the north of Henrys Fork caldera. Throughout the study area, surface displacements across the Island Park region, the ESRP, and the adjacent Basin and Range province generally reversed the movement direction in 2004, in concert with displacement reversal to uplift in the Yellowstone caldera. Crustal deformation in the general vicinity of major Basin and Range faults is interpreted to reflect diffuse extensional strain adjacent to the deeper segments of faults, rather than near-surface slip. The northeast-trending displacement zones in the ESRP and the Island Park region may indicate folding in response to converging zones of extension in the surrounding Basin and Range province. Surface displacements of the Yellowstone caldera are interpreted to reflect migration of magma or hydrothermal fluids. The inverse relation between vertical displacements in Yellowstone and its surrounding regions may reflect an upper crustal flexural response or a large-scale movement of hydrothermal fluids, though neither hypothesis is completely supported by the processed data.

1. Introduction

The Snake River Plain–Yellowstone volcano-tectonic province was created by late Cenozoic volcanism when North America migrated over a relatively stationary mantle hotspot (plume) (Morgan, 1972; Armstrong et al., 1975; Pierce and Morgan, 1992; Smith and Braile, 1993; Camp, 1995; Camp and Hanan, 2008; Shervais and Hanan, 2008). The Snake River Plain marks the older path of tectonic drift and is considered the largest actively subsiding volcanic basin in North America with regard to spatial extent and cumulative subsidence. The hotspot currently underlies the Yellowstone Plateau, and most recently erupted catastrophically ca. 640,000 years ago (Christiansen, 2001). The Yellowstone caldera, which formed at that time, is currently characterized by multiple episodes of uplift and subsidence over short-time periods (Wicks et al., 1998, 2006; Smith et al., 2006; Chang et al., 2007).

The Eastern Snake River Plain (ESRP) has existed for approximately 10 million years (Morgan and McIntosh, 2005) and its decadal to millennial subsidence is manifested by several geomorphic and geodetic indicators (Kirkham, 1931; Reilinger et al., 1977; Rodgers et al., 2002). Crustal processes that might induce subsidence of the ESRP physiographic province include: (1) heat loss leading to thermal contraction (Brott et al., 1981; Blackwell et al., 1992); (2) isostatic subsidence resulting from emplacement of dense dikes and sills (Anders and Sleep, 1992; McQuarrie and Rodgers, 1998); and (3) lower crustal flow to the adjacent Basin and Range province (McQuarrie, 1997; McQuarrie and Rodgers, 1998).

Numerous previous studies reported several remarkable manifestations of surface subsidence across the ESRP. These include (1) the immediately adjacent basins and ranges are downwarped near the ESRP, with about 1500 m decrease in surface elevation (Kirkham, 1931); (2) surface elevation of the ESRP diminishes steadily from northeast to southwest, interpreted as progressive subsidence caused by thermal contraction (Brott et al., 1981) and/or crustal loading (Anders and Sleep, 1992); (3) the ESRP and surrounding regions are characterized by axial drainage patterns, wherein tributaries flow toward the ESRP and its trunk river, which itself flows southwest along the margin of ESRP; (4) strath terraces along the southern ESRP margin are perched 900 m (late Miocene) and 200 m (early to middle Pleistocene) above the recent ESRP surface (Rodgers et al., 2002);

* Corresponding author. Tel.: +1 208 282 3439; fax: +1 208 282 4414.
E-mail address: aly@isu.edu (M.H. Aly).

0377-0273/$ – see front matter © 2009 Published by Elsevier B.V.
doi:10.1016/j.jvolgeores.2009.05.015

(5) the Lost River Trough, which is a Quaternary fluvio-lacustrine basin within the ESRP, provides evidence of long-lived but localized subsidence within the ESRP (Geslin et al., 2001); and (6) traditional land surveys indicate cm-scale decadal subsidence of the ESRP relative to its adjacent Basin and Range province (Reilinger et al., 1977).

The aforementioned geologic and geomorphic indicators imply that the ESRP subsidence is an active, ongoing process. Regional subsidence of the ESRP surface relative to the Basin and Range province and Yellowstone Plateau is, thus, anticipated. Vertical movements associated with the active Basin and Range faults, which surround the ESRP, are also probable. However, until recently it has not been possible to examine crustal motions across the broad region at issue.

Synthetic Aperture Radar Interferometry (InSAR), which is an active microwave system capable of providing a spatially dense series of crustal deformation measurements with a millimeter-level accuracy, has been applied in this study to detect and measure the spatio-temporal patterns of deformation in the ESRP and the Island Park region during 1993–2006. More specifically, the study has been conducted to test the hypothesis that the ESRP experiences short-term regional subsidence, with respect to its adjacent Basin and Range province and Yellowstone Plateau, and to investigate the possible vertical displacements associated with the active tectonics in the Basin and Range province. This InSAR investigation not only reveals the spatial and temporal patterns of crustal movements in the study area, but also has important implications for the time-transgressive nature of the complex Yellowstone system during the period of observation. This, in turn, provides a better understanding of how the lithospheric crust and mantle evolve in response to large-scale magmatism and tectonism, and it improves the understanding of earthquake cycles in the region.

2. Volcano-tectonic setting

The ESRP, which is approximately 300-km long and 80-km wide, trends northeasterly and is bounded north and south by the Basin and Range province (Fig. 1). Silicic magmatism occurred on the ESRP approximately 10 to 4 Ma ago, generally progressing to the northeast as North America migrated southwest over the Yellowstone hotspot (Armstrong et al., 1975; Pierce and Morgan, 1992; Morgan and McIntosh, 2005). The ESRP has been in the wake of the hotspot since then, and younger pulses of Pliocene-Quaternary basaltic magmatism have emanated from fissures and generated a 1-to-2 km thick layer of lava across the older silicic rocks (Kuntz et al., 1992). Lava and interbedded sediment have accumulated in the ESRP because its land surface is topographically lower than its surrounding Basin and Range province and Yellowstone Plateau.

The 1.3-Ma Henrys Fork caldera, which is situated within the Island Park region between the ESRP and the Yellowstone caldera, is nested within the southwest corner of the 2.05-Ma Huckleberry Ridge caldera (Christiansen, 2001) and shares the same rim on the southwestern sides. The Henrys Fork caldera represents the second of three major eruptive cycles on the Yellowstone Plateau and is the major contributor to the geologic history of Island Park, and is a collapse structure about 16 km in diameter (Fig. 1). The western portion of the caldera scarp is exposed; however, the eastern portion is buried under post-caldera rhyolite flows from the adjacent Yellowstone caldera to the east. The crest of the western rim of the caldera that is shared with the

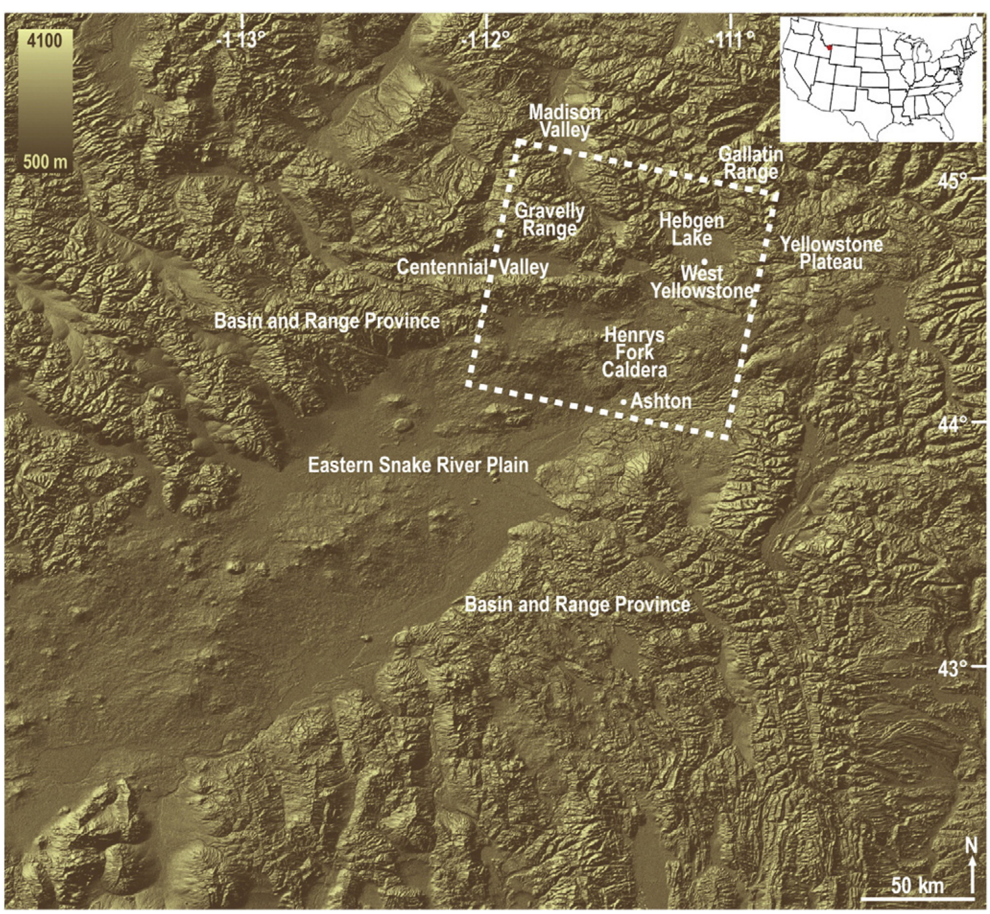

Fig. 1. Shaded relief image of the study area. The dotted white box shows the coverage of ERS data used in this interferometric investigation. All location names mentioned in the article are labeled in this figure.

Huckleberry Ridge caldera stands about 365 m above the floor of the Henrys Fork caldera. Rhyolitic pyroclastic fall and flow material erupted 1.3 Ma resulting in the collapse and formation of the Henrys Fork caldera; this was followed by smaller volume basalt and rhyolite eruptions. The final phase of volcanism here was the emplacement of the Garrit Basalt 200 ka through a series of vents in the caldera floor (Christiansen, 2001).

In the Basin and Range province north and south of the ESRP, mountains and valleys trend northwest and north, respectively. West-dipping normal faults cut all rocks and form a half-graben fault pattern. Many of these faults show evidence of Quaternary activity (Pierce and Morgan, 1992), and the most active fault scarps coincide with a parabolic zone of recent seismic activity that wraps around the ESRP (Anders et al., 1989). As they approach the ESRP and Yellowstone, the Basin and Range structures plunge beneath the onlapping volcanic rocks (Pierce and Morgan, 1992; McQuarrie and Rodgers, 1998), but the ESRP itself yields little measured seismicity. The northern part of the study area is within the Basin and Range province and shows its characteristic topography (Fig. 1). Seismicity and Global Positioning System (GPS) measurements indicate N–NNE directed extension across the region (Stickney and Bartholomew, 1987; Puskas et al., 2007), which explains the anomalous easterly trend of some ranges and basins.

3. InSAR processing and error analysis

InSAR data acquired at the C-band (5.66 cm wavelength) by the European Radar Satellites (ERS-1 and ERS-2) between 1993 and 2006 (Table 1) were used to detect and measure the recent magmatic and tectonic activity in the ESRP and the Island Park region. ERS images acquired only during the summer months were used to overcome the interferometric phase decorrelation resulting from snow accumulations. ERS pairs of short baselines (Table 1) were precisely co-registered with sub-pixel accuracy to generate differential interferograms. Then, all interferograms were multi-looked to produce outputs with homogenous pixel dimensions (40 m) in both azimuth and range directions. Ten and two looks were taken in the azimuth and range directions, respectively. Detailed information about InSAR basics and processing techniques can be found in Massonnet and Feigl (1998) and Rosen et al. (2000).

In addition to the Line-Of-Sight (LOS) deformation signals, the interferograms also contain phase noise, orbital errors, topographic signatures, and atmospheric phase delays. A nonlinear spectral filter (Goldstein and Werner, 1998) was applied to every interferogram to increase the signal to noise ratio. The DEOS precise state vectors (Scharroo and Visser, 1998) were used to compensate for orbital inaccuracies, and the residual fringes from orbital errors were corrected for by subtracting a fitted plane from each interferogram. Digital elevation data from the Shuttle Radar Topography Mission (SRTM) of 1-arc sec were used to remove the topographic contributions from all interferograms. Then, the phase error (σ) caused by the 7-m uncertainty (estimated by Farr and Kobrick, 2000) in the topographic SRTM data was calculated for each interferogram using Eq. (1).

$$\sigma = 4\pi B_{\perp} Z / \lambda \rho \sin\theta \tag{1}$$

where $B_{\perp}$ is the component of the perpendicular baseline, Z is the SRTM uncertainty, λ is the ERS wavelength, ρ is the distance from the ERS antenna to the scatterer on the ground, and θ is the incidence angle.

The calculations (Table 1) indicate that the perpendicular baseline components of ERS pairs used in this study and the estimated error in SRTM data might induce a phase error ranging between 0.21 and 0.70 rad, which is below the typical phase noise level of ERS-1 and ERS-2, on the order of ~0.70 rad (Hanssen, 2001). The topographic contribution is therefore considered negligible.

Tropospheric errors pose a considerable concern in all InSAR observations. These errors can often be eliminated, or at least decreased, by the approach of interferogram stacking. However, this approach is applicable only where constant deformation rates persist over considerable time spans. Interferogram stacking for long-time periods is thus not suitable for the study region because most of the observed deformation is nonlinear and has occurred over short time periods, as discussed below. However, interferograms spanning relatively the same time period were stacked and the outputs were averaged depending on the time interval to reduce the atmospheric effects (Table 1 and Fig. 3). Following Zebker et al. (1997), persistent phase signals were considered most likely related to real deformation, as deformation patterns usually occur at the same location in several interferograms over considerable time periods. Atmospheric artifacts, however, are not expected to occur at the same location over a considerable time span in a time series because of their dynamic nature. The degree to which atmospheric phase delays were present in the ERS acquisitions could be assessed by a pairwise comparison of interferograms (Massonnet and Feigl, 1995), and the interferograms with significant tropospheric effects were identified and discarded from further analysis.

Altitude-dependent tropospheric effects are also a major concern in areas of rough topography (>2000 m) such as the study region. The correlation between range changes and elevations is attributed to the variation between two ERS acquisitions of the average water vapor content in the lowermost atmosphere (Hanssen, 2001). The altitude-dependent atmospheric phase delay was calculated, using a linear regression analysis, and subtracted from the corrected, unwrapped interferometric phase. This correction was limited to only areas of rough topography (>2000 m) because of the significant lateral variation in local topography of the study region. The effectiveness of the utilized approach was tested using a tandem interferogram to ensure that the original signal from real deformation was not partially removed. The interferogram dated August 17, 1997–August 8, 2000 was found to be the one most impacted by altitude-dependent atmospheric effects. The area around Madison and Hebgen Faults (Fig. 2a) was significantly affected by the altitude-dependent tropospheric phase delay before correction. The corrected interferogram is shown in Fig. 2b, and the shaded relief of the same region is shown in Fig. 2c. The corrected interferometric phase of all interferograms was converted into LOS displacement in millimeters for visualization with a linear scale. Ultimately, the obtained surface displacement maps were geocoded and displayed with geographic coordinates.

Table 1
ERS raw data used in this study and calculated phase errors.

Track	Frame	Reference image			Slave image			$B_{\perp}$	σ
		Orbit	ERS	Date	Orbit	ERS	Date		
313	2709	10688	2	06051997	10979	1	21081993	099	0.46
		27722	2	08082000	12191	2	19081997	083	0.39
		28724	2	17102000	12191	2	19081997	150	0.70
		44255	2	07102003	27722	2	08082000	046	0.22
		44255	2	07102003	28724	2	17102000	139	0.65
		59285	2	22082006	48764	2	17082004	148	0.69
		59285	2	22082006	49265	2	21092004	045	0.21

Date is day, month, year.
$B_{\perp}$ is the perpendicular baseline (in meters).
σ is the phase error (in radians) caused by the topographic uncertainty of SRTM DEM.

4. Results

The obtained surface displacement maps (Fig. 3a–d) show LOS surface movements in the northeastern ESRP and the Island Park region during 1993–2006. The more recent ERS image was used as the reference for a given interferogram; therefore, positive values indicate

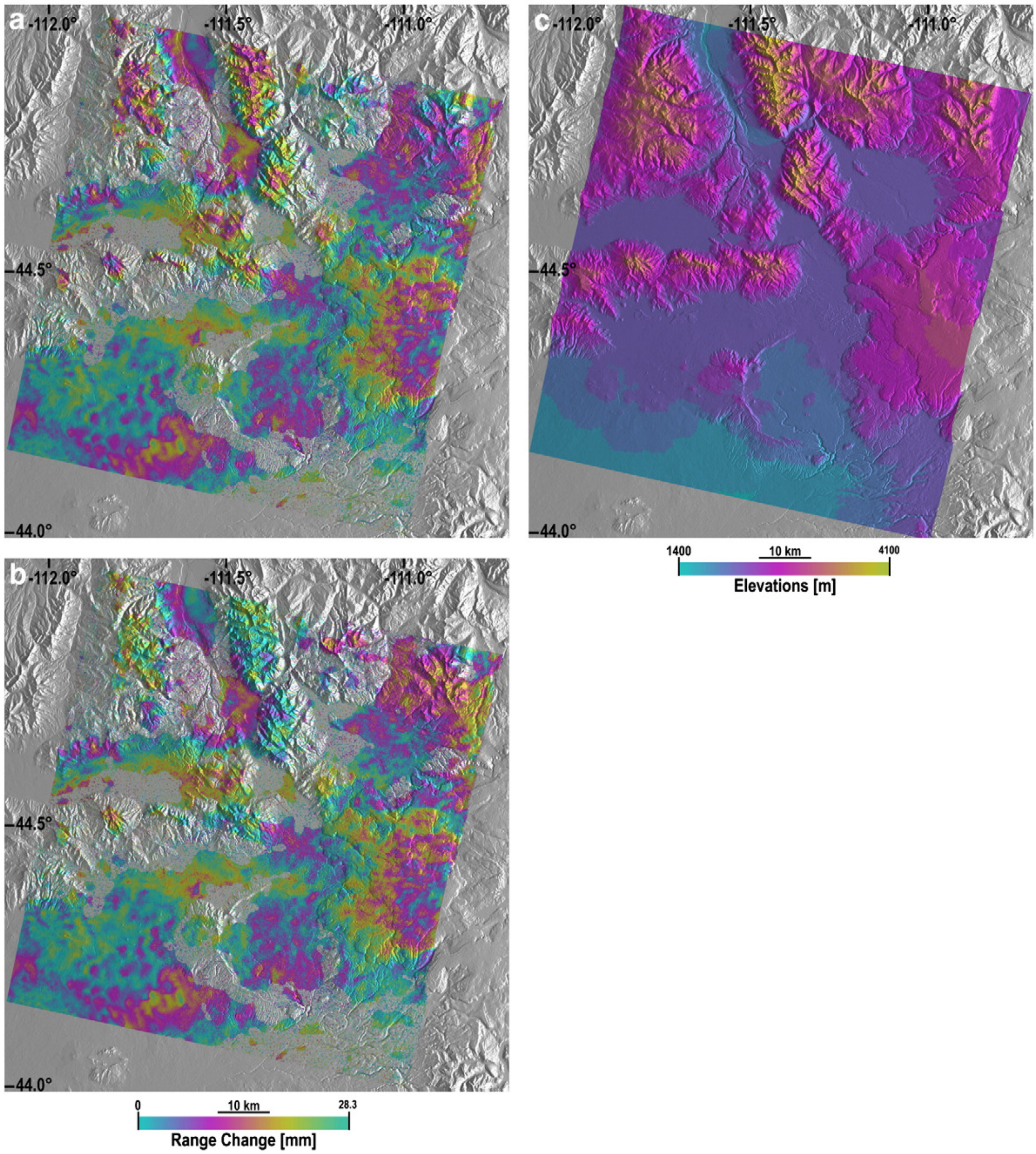

Fig. 2. ERS interferogram (August 17, 1997–August 8, 2000) (a) before and (b) after correction of the altitude-dependent atmospheric effects. (c) Shaded relief image created from the SRTM data for the same region.

movement toward the satellite and negative values indicate movement away from the satellite. Both vertical and horizontal movements are expected in the displacement maps; however, based on the ERS geometry, the vertical component of surface movements is thought to be the dominant interferometric signal in both magnitude and spatial extent.

Several regions showed non-linear crustal deformation during the periods of observations, but in most locations the displacement was not consistently up or consistently down between 1993 and 2006. Instead, most regions experienced alternating uplift and subsidence over short time spans (2–4 years). The minimum and maximum LOS surface displacements during the periods of observations ranged between −3.5 cm (away from the satellite) and +7.0 cm (toward the satellite).

The most prominent surface displacement feature in the deformation maps occurred along the western edge of Yellowstone caldera, where activity is observed in independent interferograms and marked by episodes of subsidence (-1 cm yr^{-1}) during 1997–2000 (Fig. 3b), slight subsidence during 2000–2003 (Fig. 3c), and rapid uplift ($+3$ cm yr^{-1}) during 2004–2006 (Fig. 3d). The earlier pulse of subsidence extends 10–20 km beyond the physical boundary of the caldera, whereas the most recent pulse of rapid uplift is strictly confined to the caldera itself.

Along the northwest margin of the Henrys Fork caldera, about 40 km east of the town of West Yellowstone (Fig. 1), a region of localized crustal deformation is observed. Wicks et al. (2006) first reported this as the Norris Uplift Anomaly. Our InSAR observations show that this region uplifted about $+1$ cm yr^{-1} during 1997–2000 (Fig. 3b), and during 2000–2003 it uplifted at a slower rate (about $+0.5$ cm yr^{-1}, Fig. 3c). However, during 2004–2006, this region experienced about -1.7 cm yr^{-1} of surface subsidence (Fig. 3d). All surface movements in the Norris region were, therefore, found inversely related to crustal movements within the western margin of Yellowstone caldera.

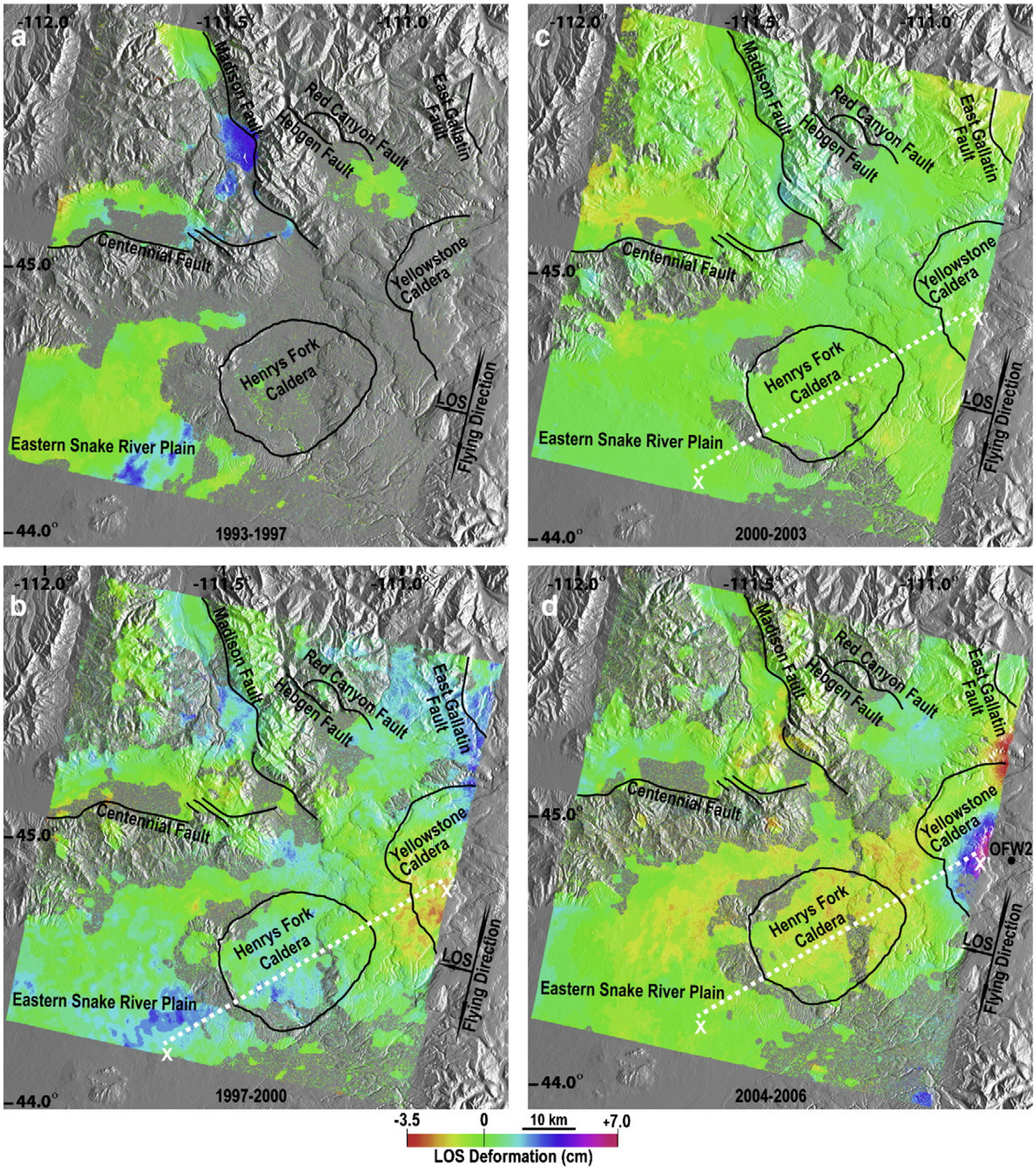

Fig. 3. LOS surface deformation across the northeastern ESRP and the Island Park region, superimposed on the hill-shaded relief image: (a) surface deformation between 21/08/1993 and 06/05/1997, (b) average deformation from the stacked interferograms dated 19/08/1997–08/08/2000 and 19/08/1997–17/10/2000, (c) average deformation from the stacked interferograms dated 08/08/2000–07/10/2003 and 17/10/2000–07/10/2003, and (d) average deformation from the stacked interferograms dated 17/08/2004–22/08/2006 and 21/09/2004–22/08/2006. The black lines indicate the major Quaternary faults in the region (U.S. Geological Survey, 2006), and the black dot marked with OFW2 indicates the location of the nearest continuous GPS station. The dotted white lines marked with X–X′ indicate the location of the deformation profiles presented in Fig. 5.

The Island Park region and the ESRP were characterized by northeast-trending zones of displacement with various extents through time. A relatively narrow zone of uplift ($+1$ cm yr^{-1}) was located just southwest of the Henrys Fork caldera, in the Pleistocene–Holocene (<15 ka) Spencer–High Point rift zone, during 1993–1997 (Fig. 3a). A similar magnitude of uplift was observed in the same location during 1997–2000, with the lateral extent of uplift extending farther northeast across the Henrys Fork caldera (Fig. 3b). Surface displacement in this region virtually ceased between 2000 and 2003 (Fig. 3c), and then during 2004–2006, a northeast-trending incoherent zone of subsidence (-1 cm yr^{-1}) developed across the Henrys Fork caldera and its immediately adjacent ESRP (Fig. 3d).

Northwest of the Island Park region is a complex structural region where the surface traces of two active normal faults, the Centennial and Madison Faults, nearly intersect at a 60° angle. Surface displacement patterns are similarly complex. The observed deformation in this region is aligned with the fault traces, but its location and magnitude vary through time. During 1993–1997, inhomogeneous uplift (approximately $+0.5$ to $+1$ cm yr^{-1}) was centered on the two basins adjacent to the faults, especially the Madison Valley. During 1997–2000, the spatial pattern of uplift (about $+0.8$ cm yr^{-1}) was shifted north and slightly west to the Gravelly Range. In the 2000–2003 period, the magnitude of uplift was decreased; however, slight uplift ($+0.5$ cm yr^{-1}) was still observable across the Madison Valley. Notably, the uplift in the region was episodically flanked by incoherent subsidence (approximately -0.7 cm yr^{-1}) in the Centennial Valley from 1997 to 2000 and in the Madison Valley from 2004 to 2006.

The northeast region of the study area, including the southernmost Gallatin Range, experienced short-term episodes of alternating uplift and subsidence. Slow subsidence (-0.5 cm yr^{-1}) followed by slow uplift ($+0.5$ cm yr^{-1}) occurred during 1993–1997 (Fig. 3a) and 1997–2000 (Fig. 3b), respectively. Zero displacement to slight subsidence (Gallatin Range) occurred during 2000–2003 (Fig. 3c). Finally, a recent episode (2004–2006) of moderate uplift ($+1$ cm yr^{-1}) occurred in the same region (Fig. 3d).

5. Discussion

The most rapidly deforming region is located in the western Yellowstone caldera margin at the eastern edge of our displacement maps, where earlier subsidence changed to rapid uplift in 2004, and in the northwestern Yellowstone caldera margin, where earlier uplift was replaced in 2004 by rapid subsidence. Geodetic GPS measurements (Fig. 4) by the continuous OFW2 station, which is located about 5 km beyond the eastern edge of our ERS images (Fig. 3d), are consistent with our InSAR-based measurements. Yellowstone deformation was previously addressed in other studies. Wicks et al. (1998) reported about -6 cm of subsidence between 1992 and 1995 in the northeast and northwest of Yellowstone caldera and about $+3$ cm of uplift in the same region during 1995–1997, using conventional InSAR techniques. Recently, Smith et al. (2006) and Chang et al. (2007) reported a new episode (2004–2006) of rapid uplift ($+7$ cm yr^{-1}), three times faster than the previously measured inflation rates in the Yellowstone caldera based on geodetic GPS and InSAR measurements. Overall, uplift and subsidence of the Yellowstone caldera were interpreted as a direct response to upper crustal migration of hydrothermal fluids and gases (Waite and Smith, 2002) or basaltic magma (Wicks et al., 2006) in and out the caldera system. Our InSAR results from the western edge of Yellowstone caldera (Fig. 3) overlap the areas described in these previous studies and reproduce their results. We concur with previous workers that the displacement observed from 1997–2006 within and on the edge of Yellowstone caldera was likely due to hydrothermal fluid or magma migration.

Our study provides new results for the region west of the Yellowstone caldera. As hypothesized previously, we anticipated that the ESRP and the Island Park region would have a pattern of widespread subsidence relative to Yellowstone and the adjacent Basin and Range province, based on the geologic record of surface subsidence over time spans >1 million year. This pattern was not observed over time spans of 2–4 years between 1993 and 2006. Instead, the ESRP and the Henrys Fork caldera were characterized by northeast-trending zones of subsidence and uplift that varied in magnitude and spatial extent every 2–4 years (Figs. 3 and 5). The lack of consistent deformation over short time scales indicates the stresses driving long-term surface subsidence–thermal contraction (Brott et al., 1981) and crustal loading (Anders and Sleep, 1992) are overwhelmed by other stresses that induce displacement at annual to decadal time scales.

What are these short-term stresses? One interpretation is based on the inverse displacement relationship between the Yellowstone caldera and the ESRP. Yellowstone subsidence from 1997 to 2000 was coeval with an elongate zone of uplift through the ESRP axial volcanic zone and the Henrys Fork caldera (Figs. 3b and 5), Yellowstone quiescence from 2000 to 2003 was coeval with ESRP and Island Park quiescence (Figs. 3c and 5), and Yellowstone uplift from 2004 to 2006 was coeval with ESRP and Island Park subsidence (Figs. 3d and 5). It is possible that upper crustal arching or sinking of the Yellowstone caldera, driven by short-term hydrothermal fluid or magma migration, resulted in a flexural response that extended approximately 100 km beyond the caldera. Flexure has been documented elsewhere in the region (McQuarrie and Rodgers, 1998) and would be an expected response adjacent to areas of significant uplift or subsidence. This hypothesis would be more strongly supported if the ESRP and the Henrys Fork caldera displacement patterns were concentric about the elliptical caldera, rather than elongate in the northeast direction.

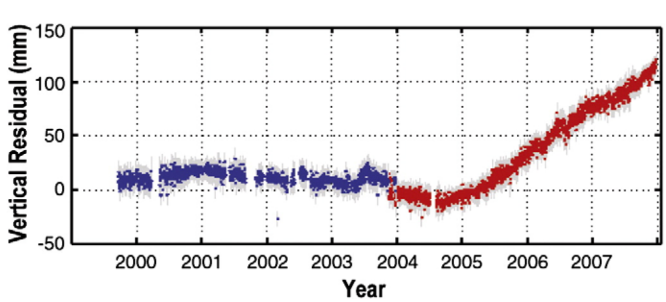

Fig. 4. Time series of the OFW2 GPS station (http://www.uusatrg.utah.edu/ Site_Info/ ofw2.html). Location of the OFW2 station is shown in Fig. 3c.

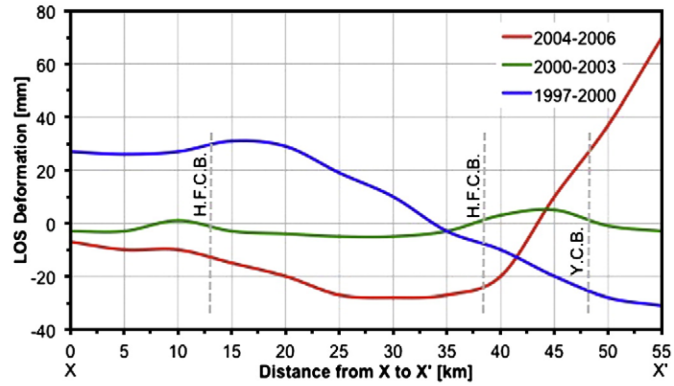

Fig. 5. Deformation profiles across the western Yellowstone caldera margin and the Island Park–ESRP region. Smoothed blue, green, and red curves represent the deformation profiles along the dotted white lines in Fig. 3b, c, and d, respectively. H.F.C.B. indicates Henrys Fork caldera boundary and Y.C.B. indicates Yellowstone caldera boundary. The distance is measured (in km) from X to X' along the indicated profile lines.

A second interpretation of the ESRP and the Henrys Fork caldera short-term displacement invokes northwest-directed shortening. The northeast-trending zones of uplift and subsidence reflect antiformal and synformal deformation that, if more consistent in space and time, would produce a series of linear northeast-trending ridges and valleys. Shortening has not been previously described in this region, and the orientation proposed here would appear to conflict with horizontal deformation immediately to the north where the Centennial Fault (and Hebgen Fault) accommodate roughly N–NNE directed extension. Only if the ESRP state of stress were considerably different than that in the Basin and Range, would this interpretation make sense. However, support for NW-directed shortening can be found in Puskas et al. (2007) who used GPS-determined displacements in the greater Yellowstone region to model regional strain rates. They found that horizontal velocities north of the Henrys Fork caldera were directed south while velocities to the south were directed west, yielding a model of ESRP contraction perpendicular to its axis. Thus, the patterns observed in the Island Park region and the ESRP (Figs. 3 and 5) could reflect cross-axis shortening characterized by very broad folds with varying hinge locations through time.

A third, somewhat related, interpretation considers the ESRP and the Henrys Fork caldera displacements to be a consequence of localized strain in the adjacent Basin and Range province. Confluence of the Madison and Centennial Faults produces a complex zone of uplift, subsidence, and horizontal displacements that might induce horizontal NW-directed contraction within the ESRP and the Henrys Fork caldera. As above, the deformation pattern in this area would reflect folds with hinges aligned parallel to the ESRP axis. Attributing the contraction to more localized strain in the Basin and Range province, rather than widespread convergence of extension vectors north and south of the ESRP, is more compatible with InSAR results to the southwest, in the central ESRP, where Aly et al. (2009) found no folds or any other pattern of surface displacement during the 1993–2000 time period.

Interpretations that do not involve tectonic stresses are thought to be less viable explanations of the observed deformation in the ESRP and the Island Park region. Magma migration was invoked to explain localized deformation within Yellowstone (Wicks et al., 2006) but this is an unlikely explanation for the more expansive, more diffuse, more irregular, and smaller magnitude of surface deformation observed in the ESRP and the Henrys Fork caldera. The three-dimensional geometry of the upper crustal magma chamber has been well characterized beneath the Yellowstone caldera (Chang et al., 2007), and it does not extend to the Henrys Fork caldera or the ESRP.

Soil swelling and shrinking also were not considered possible causes of the observed deformation in the ESRP and the region of Island Park. The National Oceanic and Atmospheric Administration (NOAA) records indicate it rained approximately 7–12 h before the older image (1997. Fig. 3b) was collected, so the Earth's surface that day might have been slightly higher in elevation due to soil swelling. Since the most recent image was used as the reference in processing, any soil swelling should yield widespread negative signals. But Fig. 3b shows widespread positive values. Similarly, it rained about 8 h before the younger image (2006, Fig. 3d) was collected. This should yield widespread positive signals, but the interferogram shows widespread negative values.

Short-term climate cycles (dry or wet) might induce variation in the groundwater table level and lead to vertical movements of the overlying rocks. The United States Geological Survey (USGS) stream flow and precipitation records indicate that 1997 was an extremely wet year while 1999–2003 was a drought period in the study area. The other years were near normal. With regard to Fig. 3b, this means the older image (1997) was acquired during a wet year and the younger image (2000) was acquired during a drought. Since the most recent image was used as the reference in our InSAR processing, this situation would yield widespread negative values in the interferogram. But Fig. 3b shows widespread positive values. With regard to Fig. 3d, both images (2004 and 2006) were taken during similar normal conditions. Then, there should be no surface change in the ESRP and the Henrys Fork caldera due to short-term climate variations; however, Fig. 3d shows widespread positive signals.

Variations in the water table levels due to groundwater pumping also were not considered a source of deformation in the ESRP-Island Park region. Only two towns in the study area, West Yellowstone (1400) and Ashton (1100), have a population over 1000. Their consumption of groundwater is, therefore, minimal and there is no correlation between town locations and areas of deformation. The only widespread agricultural irrigation in the study area is southeast of the Henrys Fork caldera — all other regions (approximately 95% of study area) are not irrigated.

Finally, a widespread hydrothermal convection system might exist in the greater Yellowstone region. Hydrothermal convection systems are common around magmatic centers and characterized by concentric patterns of altered rock and precious metal deposits (Guilbert and Park, 1986). If such a system exists in the study area, deep groundwater is expected to migrate toward the Yellowstone caldera, while shallow groundwater is expected to migrate upward and away from the Yellowstone caldera, causing a regional-scale ground deformation around the active Yellowstone caldera. Whether the complete convection system exists and whether perturbances to such a system could induce the observed patterns of surface subsidence and uplift in the ESRP-Island Park region are not known at this time.

Surface displacements in the adjacent Basin and Range province show similarly inconsistent patterns of displacement through time. Whether these patterns reflect movement along specific faults, strain distributed more diffusely in the vicinity of faults, or an inverse relation with the Yellowstone caldera is considered below.

One notable feature is that despite the presence of four active faults (Centennial, Madison, Hebgen–Red Canyon, and East Gallatin) in this part of the Basin and Range province, these faults rarely form a sharp boundary between contrasting domains of uplift or subsidence. Instead, broader domains of displacement appear to continue without interruption across the faults. One exception to this pattern is the southern hanging wall of the Madison Fault, which experienced uplift during 1993–2000 (Fig. 3a–b) in sharp contrast to its adjacent footwall. Another exception is the hanging wall of the Centennial Fault during 2000–2003 (Fig. 3c), which generally subsided (or shifted sinistrally) relative to its footwall. Otherwise, hanging walls and footwalls are not behaving as separate rigid blocks, indicating that the displacements observed in these maps are not recording near-surface slip on individual faults. However, the consistent orientation of uplift along the Madison and Centennial Faults through time suggests that short-term strain accumulation is related to fault patterns in this region. The uplift within this region could be interpreted as elastic deformation associated with interseismic strain accumulation throughout the upper crustal vicinity of the two faults. Though it does not explain the temporal variability in the location and intensity of the uplifted areas, this hypothesis can be tested through a more detailed InSAR analysis of the region in concert with the collection of a detailed GPS dataset.

Tectonic deformation might be masked or amplified by oscillations in the groundwater table. Therefore, the oscillation in the measured magnitude and change in the spatial pattern of surface deformation might be related to seasonal fluctuation of the groundwater table in the region (e.g., Bawden et al., 2001). More groundwater in the basins is expected in the spring time than the late summer time. Thus, local groundwater charge/discharge processes might have contributed, at least partially, to the detected deformation using ERS images acquired at different times of the year.

Interferometric signals in the vicinity of the Hebgen Fault did not show good coherence in any of the deformation maps from 1993 to 2004. This is due in part to rugged topography, snow cover and water surrounding the fault, which resulted in phase decorrelation along two-thirds of the fault trace. Slow uplift near the eastern end of the fault is evident between 1997 and 2004 (Fig. 3), matching GPS observations (Puskas et al., 2007) that documented uplift and north–south extension across the fault during the same approximate time period. Puskas et al. (2007) calculated about 20% of the overall displacement near the fault was due to post-seismic viscoelastic relaxation associated with the 1959 Hebgen Lake earthquake, with the remainder reflecting crustal extension.

Overall, surface displacements in this part of the Basin and Range province indicated an inverse relation with the deformation of Yellowstone caldera. Most regions of pronounced uplift or subsidence prior to 2000 show diminished movements during 2000–2003 (Fig. 3c), and then reverse their sense of displacement during 2004–2006 (Fig. 3d). These regions (Hebgen, Madison, and Centennial Valleys) are located 20–100 km northwest of the Yellowstone caldera, yet demonstrate a temporal pattern of change in harmony with changes in the caldera. The observed displacement again could be related to regional upper crustal flexure or to the lateral migration of hydrothermal gas/fluids or magma in and out the Yellowstone caldera, but the same restrictions arise as with the ESRP, as discussed above. Any rising magma sourced from Yellowstone is believed to be driven directly upward by buoyancy forces, not laterally for tens of kilometers through the shallow crust. Still, we are unable to provide a more likely interpretation than flexure or hydrothermal fluids migration to explain the inverse displacement relations between Yellowstone and the adjacent Basin and Range province.

6. Conclusions

This study addresses crustal deformation in the ESRP, the Island Park region, and adjacent northern Basin and Range province using

ERS InSAR data acquired at the C-band (5.66 cm wavelength) during 1993–2006. InSAR observations show that the study area experienced non-linear, episodic crustal movements, with a minimum of −3.5 cm and a maximum of +7.0 cm in the LOS direction, during the period of observation.

Surface displacements observed in the general vicinity of major Basin and Range faults are most likely related to tectonic activity associated with diffuse extensional strain adjacent to the deeper segments of faults, rather than near-surface slip. The northeast elongation of displacement zones in the ESRP and the Henrys Fork caldera may reflect northwest-directed contraction due to converging zones of extension, or possibly more localized strain patterns, in the surrounding Basin and Range province. The complex Yellowstone volcanic system is well-known for its alternating episodes of uplift and subsidence, and volume changes in the magma chamber or migrating hydrothermal fluids are most likely responsible for its alternating up and down displacements. The recognition that interferometric signals in the Island Park region, the northeastern ESRP, and the Basin and Range province are not only variable in time, but also inversely related to signals in the Yellowstone caldera, may indicate a direct connection between the driving forces of surface deformation in the three adjacent regions. The inverse relation could be interpreted as a flexure response of the Island Park-ESRP region to deformation of the Yellowstone caldera. Alternatively (or in addition to flexure), the inverse relation could reflect a lateral migration of hydrothermal fluids to and from the Yellowstone caldera as the caldera expands and contracts.

Acknowledgements

This study was funded by the NASA EPSCoR grant #NCC5-577 and the NOAA grant #NA06OAR4600124 awarded to Idaho State University. ERS InSAR data were provided at the production cost by the European Space Agency (ESA) under a Category-1 Proposal #4242. The SRTM digital elevation data were obtained from NASA JPL. The authors would like to thank the editor and two anonymous reviewers for their constructive comments and suggestions, which improved the quality of this manuscript significantly.

References

Aly, M.H., Rodgers, D.W., Thackray, G.D., 2009. Differential SAR Interferometry to investigate surface deformation of the Eastern Snake River Plain, Idaho, USA. Journal of Geology 117, 103–108. doi:10.1086/595504.

Anders, M.H., Sleep, N.H., 1992. Magmatism and extension: the thermal and mechanical effects of the Yellowstone hotspot. Journal of Geophysical Research 97, 15379–15394.

Anders, M.H., Geissman, J.W., Piety, L.A., Sullivan, J.T., 1989. Parabolic distribution of circum-eastern Snake River Plain seismicity and latest Quaternary faulting, migratory pattern and association with the Yellowstone hotspot. Journal of Geophysical Research 94, 1589–1621.

Armstrong, R.L., Leeman, W.P., Malde, H.E., 1975. K–Ar dating, Quaternary and Neogene volcanic rocks of the Snake River Plain, Idaho. American Journal of Science 275, 225–251.

Bawden, G.W., Thatcher, W., Stein, R.S., Hudunt, K.W., Peltzer, G., 2001. Tectonic contraction across Los Angeles after removal of groundwater pumping effects. Nature 412, 812–815.

Blackwell, D.D., Kelley, S., Steele, J.L., 1992. Heat flow modeling of the Snake River Plain, Idaho. U.S. Department of Energy Report for contract DE-AC07-761DO1570, p. 109.

Brott, C.A., Blackwell, D.D., Ziagos, J.P., 1981. Thermal and tectonic implications of heat flow in the eastern SRP, Idaho. Journal of Geophysical Research 86 (B12), 709–734.

Camp, V.E., 1995. Mid-Miocene propagation of the Yellowstone mantle plume head beneath the Columbia River Basalt source region. Geology 23, 435–438.

Camp, V.E., Hanan, B.B., 2008. A plume-triggered delamination origin for the Columbia River Basalt Group. Geosphere 4, 480–495.

Chang, W.L., Smith, R.B., Wicks, C., Farrell, J.M., Puskas, C.M., 2007. Accelerated uplift and magmatic intrusion of the Yellowstone caldera, 2004 to 2006. Science 318, 952–956.

Christiansen, R.L., 2001. The Quaternary and Pliocene Yellowstone Plateau volcanic field of Wyoming, Idaho, and Montana. United States Geological Survey Professional Paper 729-G, 145.

Farr, T.G., Kobrick, M., 2000. Shuttle Radar Topography Mission products as a wealth of data. EOS, Transactions of the American Geophysical Union 81 (48), 583–585.

Geslin, J.K., Link, P.K., Riesterer, J.W., Kuntz, M.A., Fanning, C.M., 2001. Pliocene and Quaternary stratigraphic architecture and drainage systems of the Big Lost Trough, northeastern Snake River Plain, Idaho. In: Link, P.K., Mink, L.L. (Eds.), Geology, Hydrogeology, and Environmental Remediation, Idaho National Engineering and Environmental Laboratory, Eastern Snake River Plain, Idaho. GSA Special Paper 353, 11–27.

Goldstein, R., Werner, C., 1998. Radar interferogram filtering for geophysical applications. Geophysical Research Letters 25 (21), 4035–4038.

Guilbert, J.M., Park Jr., C.F., 1986. The Geology of ore deposits. Waveland Press, Long Grove, Illinois.

Hanssen, R., 2001. Radar Interferometry: Data Interpretation and Error Analysis. Kluwer Academic Publishers, Boston, p. 308.

Kirkham, V.R.D., 1931. Snake River downwarp. Journal of Geology 39, 456–487.

Kuntz, M.A., Covington, H.R., Schorr, L.J., 1992. An overview of basaltic volcanism of the ESRP, Idaho. In: Link, P.K., Kuntz, M.A., Platt, L.P. (Eds.), Regional geology of eastern Idaho and western Wyoming: Geological Society of America, vol. 179, pp. 227–267.

Massonnet, D., Feigl, K., 1995. Discrimination of geophysical phenomena in satellite radar interferograms. Geophysical Research Letters 22 (12), 1537–1540.

Massonnet, D., Feigl, K.L., 1998. Radar interferometry and its application to changes in the Earth's surface. Reviews of Geophysics 36 (4), 441–500.

McQuarrie, N., 1997. Crustal flexure adjacent to the eastern Snake River Plain, Idaho. Idaho State University, M.S. Thesis. 87.

McQuarrie, N., Rodgers, D.W., 1998. Subsidence of a volcanic basin by flexure and lower crustal flow: the eastern Snake River Plain, Idaho. Tectonics 17, 203–220.

Morgan, W.J., 1972. Plate motions and deep mantle convection. Geological Society of America 132, 7–22.

Morgan, L.A., McIntosh, W.C., 2005. Timing and development of the Heise volcanic field, Snake River Plain, Idaho western USA. Geological Society of America 117, 288–301.

Pierce, K.L., Morgan, L.A., 1992. The track of the Yellowstone hotspot; volcanism, faulting and uplift. In: Link, P.K., Kuntz, M.A., Platt, L.B. (Eds.), Regional Geology of Eastern Idaho and Western Wyoming: Geological Society of America Mem, vol. 179, pp. 1–53.

Puskas, C.M., Smith, R.B., Meertens, C.M., Chang, W.L., 2007. Crustal deformation of the Yellowstone-Snake River Plain volcanic system: campaign and continuous GPS observations, 1987–2004. Journal of Geophysical Research 112 (B03401). doi:10.1029/2006JB004325.

Reilinger, R.E., Citron, G.P., Brown, L.D., 1977. Recent vertical crustal movements from precise leveling data in southwestern Montana, western Yellowstone National Park and the Snake River Plain. Journal of Geophysical Research 82, 5349–5359.

Rodgers, D.W., Ore, H.T., Bobo, R., McQuarrie, N., Zentner, N., 2002. Extension and subsidence of the eastern Snake River Plain. In: Bonnichsen, B., White, C., McCurry, M.O. (Eds.), Tectonic and magmatic evolution of the Snake River Plain volcanic province: Idaho Geological Survey Bulletin, vol. 30, pp. 121–160.

Rosen, P.A., Hensley, S., Joughin, I.R., Li, F.K., Madsen, S.N., Rodríguez, E., Goldstein, R.M., 2000. Synthetic Aperture Radar Interferometry. Proceedings of the IEEE 88 (3), 333–382.

Scharroo, R., Visser, P., 1998. Precise orbit determination and gravity field improvement for the ERS satellites. Journal of Geophysical Research 103 (C4), 8113–8127.

Shervais, J.W., Hanan, B.B., 2008. Lithospheric topography, tilted plumes, and the track of the Snake River–Yellowstone hot spot. Tectonics 27, TC5004. doi:10/1029/2007/TC002181.

Smith, R.B., Braile, L.W., 1993. Topographic signature, space–time evolution, and physical properties of the Yellowstone–Snake River Plain volcanic system: the Yellowstone hotspot. In: Sn oke, A.W., Steidtmann, J.R., Roberts, S.M. (Eds.), Geology of Wyoming: Geological Survey of Wyoming, vol. 5, pp. 694–754.

Smith, R.B., Jordan, M., Puskas, C.M., Farrell, J., Waite, G.P., 2006. Origin and evolution of the Yellowstone hotspot from seismic-GPS imaging and geodynamic modeling. EOS, Transactions of the American Geophysical Union 87 (52) S54A-06.

Stickney, M.C., Bartholomew, M.J., 1987. Seismicity and late Quaternary faulting of the northern Basin and Range province, Montana and Idaho. Bulletin of the Seismological Society of America 77, 1602–1625.

U.S. Geological Survey, 2006. Quaternary fault and fold database for the United States. accessed May 19, 2008, from USGS web site: http//earthquakes.usgs.gov/regional/qfaults/.

Waite, G.P., Smith, R.B., 2002. Seismic evidence for fluid migration accompanying subsidence of the Yellowstone caldera. Journal of Geophysical Research 107 (B9), 2177. doi:10.1029/2001JB000586.

Wicks, C., Thatcher, W., Dzurisin, D., 1998. Migration of fluids beneath Yellowstone caldera inferred from Satellite Radar Interferometry. Science 282, 458–462.

Wicks, C., Thatcher, W., Dzurisin, D., Svarc, J., 2006. Uplift, thermal unrest and magma intrusion at Yellowstone caldera. Nature 440, 72–75.

Zebker, H., Rosen, P., Hensley, S., 1997. Atmospheric effects in interferometric synthetic aperture radar surface deformation and topographic maps. Journal of Geophysical Research 102 (B4), 7547–7563.